Dipole Effects on Cation−π Interactions: Absolute Bond Dissociation Energies of Complexes of Alkali Metal Cations to *N*-methylaniline and *N,N*-dimethylaniline

Nuwan Hallowita,[†] Damon R. Carl,[‡] P. B. Armentrout,[‡] and M. T. Rodgers*,[†]

Department of Chemistry, Wayne State University, Detroit, Michigan 48202, and Department of Chemistry, University of Utah, Salt Lake City, Utah 84112

Received: January 16, 2008; Revised Manuscript Received: May 24, 2008

Threshold collision-induced dissociation of $M^+(nMA)_x$ with Xe is studied using guided ion beam mass spectrometry, where *n*MA = *N*-methylaniline and *N,N*-dimethylaniline and $x = 1$ and 2. M^+ includes the following alkali metal cations: Li^+, Na^+, K^+, Rb^+, and Cs^+. In all cases, the primary dissociation pathway corresponds to the endothermic loss of an intact *n*MA ligand. The primary cross section thresholds are interpreted to yield 0 and 298 K bond dissociation energies (BDEs) for $(nMA)_{x-1}M^+-(nMA)$ after accounting for the effects of multiple ion−neutral collisions, the internal and kinetic energy distributions of the reactants, and the dissociation lifetimes. Density functional theory calculations at the B3LYP/6-31G* level of theory are used to determine the structures of these complexes, which are also used in single-point calculations at the MP2(full)/6-311+G(2d,2p) level to determine theoretical BDEs. The results of these studies are compared to previous studies of the analogous $M^+(aniline)_x$ complexes to examine the effects of methylation of the amino group on the binding interactions. Comparisons are also made to a wide variety of cation−π complexes previously studied to elucidate the contributions that ion−dipole, ion−induced-dipole, and ion−quadrupole interactions make to the overall binding.

Introduction

Noncovalent interactions play a variety of roles in many areas of modern chemistry and biochemistry. Cation−π interactions are among the important noncovalent binding forces that also include salt bridges, hydrophobic interactions, hydrogen bonds, and π-stacking interactions. All play roles in determining the structures and controlling the functions of biological macromolecules. Many studies suggest the involvement of cation−π interactions in molecular recognition processes[1–9] and ion channels,[10–13] and hence, Na^+ and K^+ have been widely studied because they are the most biologically important alkali metal cations.[14,15] Cation−π interactions also influence the stability of proteins and protein−DNA complexes.[16–18] Finally, it is believed that through the appropriate addition of substituents to the aromatic ring, the strength of cation−π interactions between a metal cation and π-binding ligands can be tailored so as to devise new chemical separation strategies for the removal of unnecessary and toxic species from environmental sources such as water streams.[19]

Studies of alkali metal cations binding to model aromatic ligands and characterization of these metal−ligand interactions in the gas phase is an important and essential part of building a database of information concerning the nature and strength of cation−π interactions. To obtain a complete picture of cation−π interactions, the contributions that the fundamental intermolecular forces, i.e., ion−quadrupole, ion−induced-dipole, and ion−dipole interactions, make to these interactions need to be elucidated. Dougherty and co-workers stated that electrostatic interactions play a prominent role in cation−π interactions.[20] Their ab initio calculations of 11 Na^+ complexes suggested that the electrostatic energy is about 40−60% of the total interaction energy of most complexes.[21] They further reported that the linear relationship between the calculated binding energies and the electrostatic contributions of the systems studied emphasizes that variations in the binding energy are completely accounted for by the electrostatic term.[21] Theoretical studies have shown that polarization is also an important factor in determining the strength of cation−π interactions because the cation produces a strong electric field.[22,23]

Several previous experimental studies of the interactions between the alkali metal cations and model aromatic ligands, i.e., benzene (B),[24,25] toluene (T),[26] fluorobenzene (F),[27] phenol (P),[28] anisole (S),[29] naphthalene (N),[30] indole (I),[31] pyrrole (R),[32–34] and aniline (A),[35] have been reported. Analyses of the trends in the bond dissociation energies (BDEs) for these systems suggest that cation−π interactions are dominated by ion−quadrupole interactions and enhanced by ion−induced-dipole interactions. However, the direct contributions that ion−dipole interactions contribute to the strength of cation−π interactions has not yet been assessed because in the model systems examined, only aniline, $C_6H_5NH_2$, possesses a component of its dipole moment perpendicular to the plane of the aromatic ring. In this study, we examine cation−π interactions of *N*-methylaniline, $C_6H_5NHCH_3$ (NMA),and *N,N*-dimethylaniline, $C_6H_5N(CH_3)_2$ (NNDMA) with Li^+, Na^+, K^+, Rb^+, and Cs^+ using quantitative threshold collision-induced dissociation (CID) methods to determine the influence of ion−dipole interactions on cation−π interactions. The structures of B, A, NMA, and NNDMA along with their calculated (and measured)[36,37] dipole moments and molecular polarizabilities are shown in Figure 1.

Experimental Section

General Procedures. Guided ion beam tandem mass spectrometers that have been described in detail previously[38–40] were

* Corresponding author. E-mail: mrodgers@chem.wayne.edu.
† Wayne State University.
‡ University of Utah.

10.1021/jp800434v CCC: $40.75
Published on Web 08/13/2008

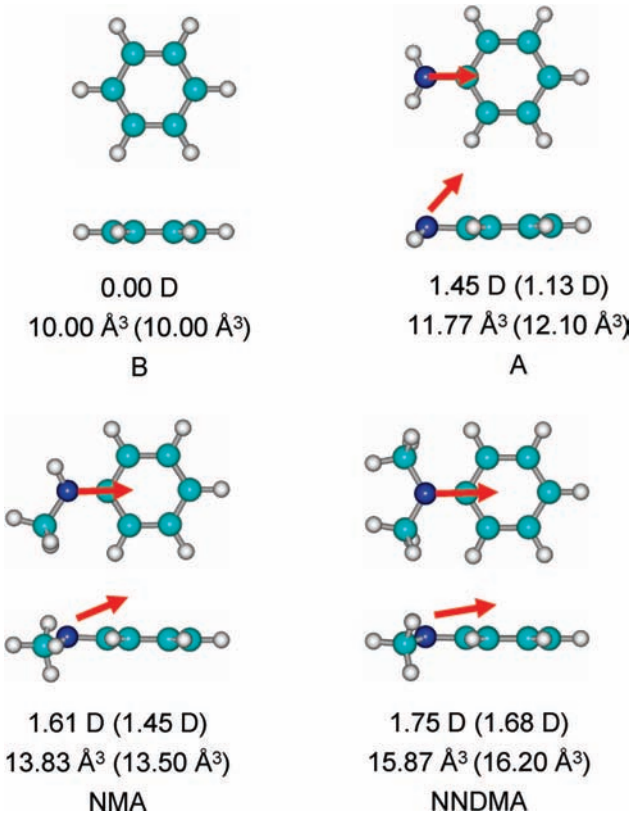

Figure 1. Geometry optimized structures of B, A, NMA, and NNDMA. Properly scaled and oriented dipole moments in Debye are shown as arrows and determined from theoretical calculations performed here. Calculated isotropic molecular polarizability volumes are also shown. Measured dipole moments and polarizability volumes are given in parentheses and taken from refs 36 and 37.

used to measure kinetic-energy-dependent cross sections for CID of 20 $M^+(n\text{MA})_x$ complexes, where $M^+ = Li^+$, Na^+, K^+, Rb^+, and Cs^+, nMA = NMA and NNDMA, and $x = 1$ and 2. These complexes are generated in a flow tube ion source by condensation of the alkali metal cation and neutral nMA ligand(s). The complexes are collisionally stabilized and thermalized by $>10^5$ collisions with the He and Ar bath gases such that the internal energies of cations emanating from the source region are assumed to be well described by a Maxwell−Boltzmann distribution at room temperature. The ions are effusively sampled from the source, focused, and accelerated into a magnetic sector for mass analysis. Mass-selected ions are decelerated to a desired kinetic energy and focused into an octopole ion beam guide. The octopole passes through a static gas cell containing Xe at low pressure (0.05−0.20 mTorr) to ensure that multiple ion−neutral collisions are improbable. The octopole ion beam guide acts as an efficient radial ion trap. Therefore, loss of scattered reactant and product ions in the octopole region is almost entirely eliminated.[41–43] Xe is used here and in general for all of our CID measurements, because it is heavy and polarizable and therefore leads to more efficient kinetic-to-internal energy transfer in the CID process.[44–46] Remaining reactant and product ions drift to the end of the octopole, where they are focused into a quadrupole mass filter for mass analysis and subsequently detected with a secondary electron scintillation detector and standard pulse counting techniques.

Ion intensities are converted to absolute cross sections using a Beers' law analysis as described previously.[39] Errors in pressure measurement and in the length of the interaction region lead to ±20% uncertainties in the absolute cross-section magnitudes. Relative uncertainties are approximately ± 5%.

Ion kinetic energies in the laboratory frame, E_{lab}, are converted to energies in the center of mass frame, E_{CM}, by using the formula $E_{CM} = E_{lab}m/(m + M)$, where M and m are the masses of the ionic and neutral reactants, respectively. All energies reported below are in the center-of-mass frame unless otherwise noted. The absolute zero and distribution of ion kinetic energies are determined by using the octopole ion guide as a retarding potential analyzer as previously described.[39] The distribution of ion kinetic energies is nearly Gaussian with a fwhm between 0.2 and 0.5 eV (laboratory) for these experiments. The uncertainty in the absolute energy scale is ±0.05 eV (lab).

Because multiple ion−neutral collisions can influence the shape of CID cross sections, particularly in the threshold region, the CID cross section for each complex was measured twice at three nominal pressures (0.05, 0.10, and 0.20 mTorr). Data free from pressure effects are obtained by extrapolating to zero reactant pressure, as described previously.[47] The zero-pressure-extrapolated cross sections subjected to thermochemical analysis are therefore the result of single bimolecular encounters.

Theoretical Calculations. To obtain model structures, vibrational frequencies, rotational constants, and energetics for the neutral nMA ligands and $M^+(n\text{MA})_x$ complexes, electronic structure calculations were performed using Gaussian 98 and 03.[48] Geometry optimizations were performed at the B3LYP/6-31G* level[49,50] for the complexes to Li^+, Na^+, and K^+. For complexes containing Rb^+ and Cs^+, geometry optimizations were performed using the B3LYP functional with a hybrid basis set (HW-6-31G*) in which the effective core potentials (ECPs) and valence basis sets of Hay and Wadt were used to describe the alkali metal cation,[51,52] whereas 6-31G* basis sets were used for the C, N, and H atoms. As suggested by Glendening et al.,[53] a single polarization (d) function was added to the Hay−Wadt valence basis set for Rb and Cs, with exponents of 0.24 and 0.19, respectively. Vibrational analyses of the geometry-optimized structures were performed to determine the vibrational frequencies of the optimized species for use in modeling of the CID data. The calculated frequencies were scaled by a factor of 0.9804.[54] The scaled vibrational frequencies are available as Supporting Information in Table 1S. Table 2S lists the rotational constants for the ground-state conformations. Single-point calculations were performed at the MP2(full)/6-311+G(2d,2p) and MP2(full)/HW-6-311+G(2d,2p) levels of theory using the B3LYP/6-31G* and B3LYP/HW-6-31G* optimized geometries, respectively.

Because the smaller size of the Li^+ cation results in shorter metal−ligand bond distances, greater electronic distortion of the nMA ligand occurs upon complexation. As a result, larger basis sets are necessary to accurately describe the $Li^+(n\text{MA})$ complexes. Therefore, geometry optimizations and single-point calculations for the Li^+(A), Li^+(NMA), and Li^+(NNDMA) complexes were performed at the MP2(full)/cc-pVDZ and MP2(full)/aug-cc-pVTZ levels of theory, respectively. However, when the metal−ligand bond distances become shorter, the closed-shell core electrons on the metal cation repulsively interact with the closed-shell ligand. This effect can be considered by permitting the core electrons of the metal cation to polarize away from the ligand and correlate with the ligand electrons. However, standard basis sets do not include correlation functions on the core electrons of Li^+.[55] Therefore, the correlation consistent polarized core/valence basis sets developed by Dunning[56,57] were used to describe Li^+, i.e., the cc-pCVDZ basis set for geometry optimization and the cc-pCVTZ basis set for

the single point calculations, and will be referred to as cc-pVDZ(Li−C) and aug-cc-pVTZ(Li−C), respectively. Additionally, G3 calculations for the $Li^+(n\text{MA})$ systems were performed to obtain further comparisons.

To obtain accurate BDEs for these systems, zero-point energy (ZPE) corrections were applied, and basis set superposition errors (BSSEs) were subtracted from the computed dissociation energies in the full counterpoise correction.[58,59] Our previous work[55] shows that correcting for BSSE in the MP2(full)/aug-cc-pVTZ(Li−C) calculations reduces the accuracy of the thermochemical results; hence, no counterpoise corrections were made for these calculations.

As a result of the multiple favorable alkali metal cation binding sites to these ligands, several low-energy conformations of these species are possible. Therefore, we carefully consider various possible conformations of the $M^+(n\text{MA})_x$ complexes to determine their relative stabilities and the ground-state conformations. In order to quantify and visualize the electronic properties of *n*MA, and thereby better understand preferences for various binding modes, the isotropic molecular polarizabilities of the neutral π-ligands examined here and in previous TCID studies[24–35] of cation−π interactions (i.e., B, A, NMA, NNDMA, T, P, S, I, and R) were calculated at the PBE0/6-311+G(2d,2p) level of theory. This level of theory has been shown to accurately reproduce experimental polarizabilities.[60] Electrostatic potential (ESP) maps for the *n*MA ligands were also calculated. For visualization, the ESP is mapped onto an isosurface of the total SCF electron density (0.005 au for the maps generated in this work). The ESP maps generated are color-coded according to potential with the regions of greatest ESP shown in red and those with the least shown in blue.

Thermochemical Analysis. The threshold regions of the CID cross sections are modeled by using eq 1,

$$\sigma(E) = \sigma_0 \sum_i g_i (E + E_i - E_0)^n / E \qquad (1)$$

where σ_0 is an energy-independent scaling factor, E is the relative translational energy of the reactants, E_0 is the threshold for reaction of the ground electronic and ro-vibrational state, and n is an adjustable parameter that describes the efficiency of kinetic to internal energy transfer.[40] The summation is over the ro-vibrational states of the reactant ions, i, where E_i is the excitation energy of each ro-vibrational state, and g_i is the population of those states ($\Sigma g_i = 1$). The relative reactivity of all ro-vibrational states, as reflected by σ_0 and n, is assumed to be equivalent.

The Beyer−Swinehart algorithm[61–63] is used to evaluate the density of the ro-vibrational states, and the relative populations, g_i, are calculated for a Maxwell−Boltzmann distribution at 298 K, the internal temperature of the reactants. The average vibrational energies at 298 K of the *n*MA ligands and $M^+(n\text{MA})_x$ complexes are given in Table 1S of the Supporting Information. We have estimated the sensitivity of our analysis to the deviations from the true frequencies by increasing and decreasing the calculated frequencies (scaled by 0.9804) by 10%. For the complexes to Rb^+ and Cs^+, 20% variations were applied. The corresponding change in the average vibrational energy is assumed to be an estimate of one standard deviation of the uncertainty in the vibrational energy (Table 1S in the Supporting Information). For the bis-ligated systems, we also explicitly tested whether the vibrational motion corresponding to relative rotations of the two ligands about the symmetry axis (the lowest-frequency vibration in all cases) should be treated as a rotor instead. Such a treatment changed the interpretation of the data by much less than the stated uncertainties (on the order of 1 meV).

We also consider the possibility that collisionally activated complex ions do not dissociate on the time scale of our experiment ($\sim 10^{-4}$ s) by including statistical theories for unimolecular dissociation, specifically Rice−Ramsperger−Kassel−Marcus (RRKM) theory, into eq 1, as described in detail elsewhere.[64,65] The ro-vibrational frequencies appropriate for the energized molecules and the transition states (TSs) leading to dissociation are given in Tables 1S and 2S in the Supporting Information. In our analyses, we assume that the TSs are loose and product-like because the interaction between the alkali metal cation and the *n*MA ligand(s) is largely electrostatic (ion−quadrupole, ion−dipole, and ion−induced-dipole interactions). Thus, the most appropriate model for the TS is a loose phase space limit (PSL) model located at the centrifugal barrier for the interaction of $M^+(n\text{MA})_{x-1}$ with *n*MA, as described in detail elsewhere.[64]

The model represented by eq 1 is expected to be appropriate for translationally driven reactions[66] and has been found to reproduce CID cross sections well in previous studies. The model is convoluted with the kinetic energy distributions of both reactants, and a nonlinear least-squares analysis of the data is performed to give optimized values for the parameters σ_0, E_0, and n. The error associated with the measurement of E_0 is estimated from the range of threshold values determined for the zero-pressure-extrapolated data sets, variations associated with uncertainties in the vibrational frequencies (±10%/± 20% scaling) and the error in the absolute energy scale, ± 0.05 eV (lab). For analyses that include the RRKM lifetime analysis, the uncertainties in the reported E_0(PSL) values also include the effects of increasing and decreasing the time assumed available for dissociation by a factor of 2.

Equation 1 explicitly includes the internal energy of the ion, E_i. All energy available is treated statistically because the internal (rotational and vibrational) energy of the reactants is redistributed throughout the $M^+(n\text{MA})_x$ complex upon collision with Xe. Because the CID processes examined here are simple noncovalent bond fission reactions, the E_0(PSL) values determined by analysis with eq 1 can be equated to 0 K BDEs.[67,68]

Results

Cross Sections for CID. Experimental cross sections were obtained for the interaction of Xe with 20 $M^+(n\text{MA})_x$ complexes, where *n*MA = NMA and NNDMA, $x = 1$ and 2, and $M^+ = Li^+$, Na^+, K^+, Rb^+, and Cs^+. Figure 2 shows representative data for the $Na^+(\text{NMA})_x$ complexes. The other $M^+(n\text{MA})_x$ complexes exhibit similar behavior and are shown in Figure 1S of the Supporting Information. Over the range of collision energies examined, two types of processes are observed, simple CID resulting in the loss of intact *n*MA ligands and ligand exchange with Xe. The dominant reaction pathway observed at all energies for all of the $M^+(n\text{MA})_x$ complexes is the loss of a single intact *n*MA ligand in the CID reactions 2.

$$M^+(n\text{MA})_x + \text{Xe} \rightarrow M^+(n\text{MA})_{x-1} + n\text{MA} + \text{Xe} \qquad (2)$$

Dissociation of a second *n*MA ligand is observed for the bis-complexes at elevated energies. The shape of the CID cross sections confirms that these products are formed sequentially from the primary product; i.e., the cross section for formation of $M^+(n\text{MA})$ begins to decline as the secondary product, M^+, begins to appear. Ligand exchange to form M^+Xe is observed for most of the $M^+(n\text{MA})$ complexes. It is likely that this process

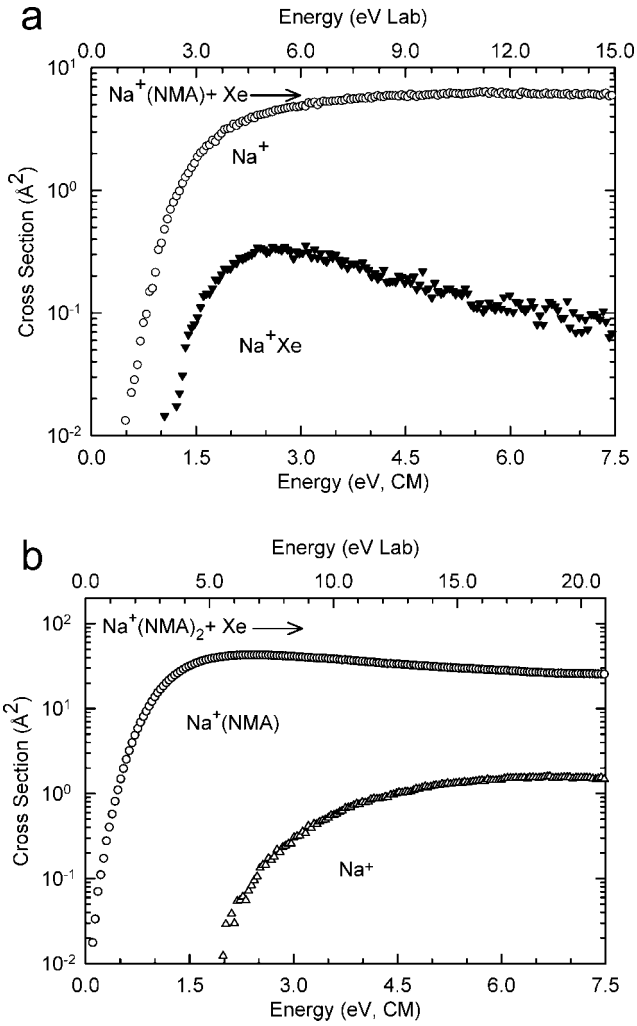

Figure 2. Cross sections for CID of $Na^+(NMA)_x$ complexes, where $x = 1$ and 2 (parts a and b, respectively), with Xe as a function of collision energy in the center-of-mass frame (lower x-axis) and laboratory frame (upper x-axis). Data are shown for a Xe pressure of 0.2 mTorr.

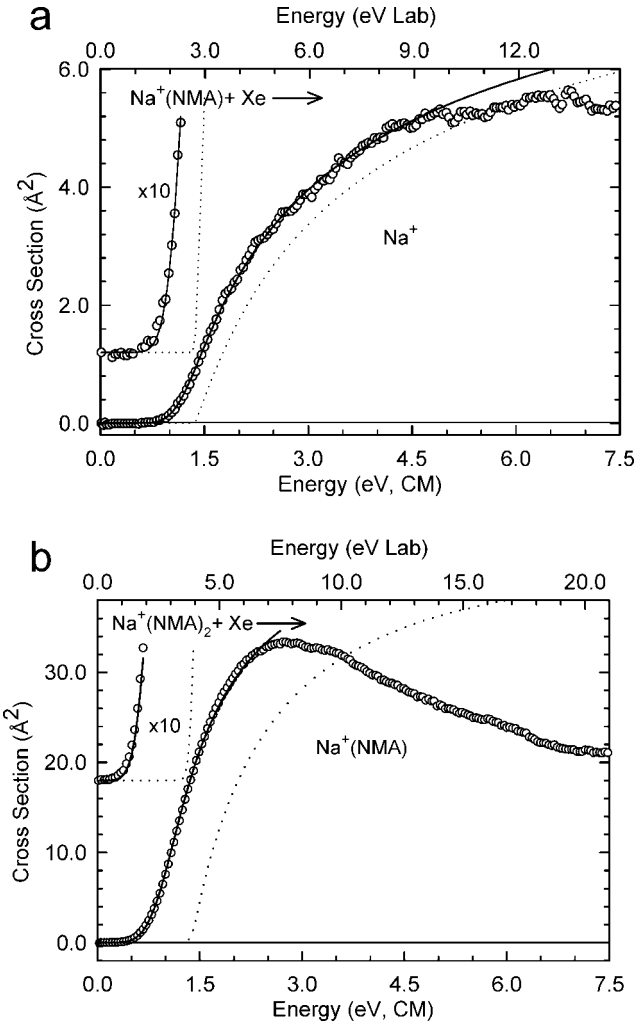

Figure 3. Zero-pressure-extrapolated cross sections for CID of $Na^+(NMA)_x$ complexes, where $x = 1$ and 2 (parts a and b, respectively), with Xe in the threshold region as a function of kinetic energy in the center-of-mass frame (lower x-axis) and laboratory frame (upper x-axis). Solid lines show the best fits to the data by using eq 1 convoluted over the kinetic and internal energy distributions of the reactants. Dotted lines show the model cross sections in the absence of experimental kinetic energy broadening for reactants with an internal energy corresponding to 0 K.

occurs for all complexes but that the signal-to-noise in the other systems was not sufficient to differentiate the ligand exchange product(s) from background noise.

Threshold Analysis. The model of eq 1 was used to analyze the thresholds for reactions 2 in 20 $M^+(n\text{MA})_x$ systems. The results of these analyses are given in Table 1. Representative fits using eq 1 for the $Na^+(NMA)_x$ complexes are shown in Figure 3. Analyses for the other $M^+(n\text{MA})_x$ complexes are shown in Figure 2S of the Supporting Information. Experimental cross sections for the primary dissociation processes of the $M^+(n\text{MA})_x$ complexes are accurately reproduced using a loose PSL TS model.[64] This model has been shown to provide the most accurate determination of kinetic shifts for CID of electrostatically bound complexes.[24,69] The data are accurately reproduced over energy ranges exceeding 1.0 eV and over cross-section magnitudes of a factor of at least 100 for all complexes except $Rb^+(n\text{MA})_x$ and $Cs^+(n\text{MA})_x$ because the primary product cross sections are already nonzero at 0 eV in these complexes. Threshold values, E_0 and E_0(PSL), obtained from analyses of data without and including explicit consideration of lifetime effects are also included in Table 1. The difference between these threshold values, the kinetic shift, is also given in Table 1. The kinetic shifts observed for these systems vary from 0.01 to 0.56 eV. The kinetic shifts decrease with increasing size of the cation, from Li^+ to Cs^+, for both the mono- and bis-complexes. For all of the metal cations, the kinetic shift increases from the mono- to the corresponding bis-complex. These behaviors are easily understood because the observed kinetic shift should directly correlate with the density of states of the complex at threshold, which depends upon the measured BDE and the number of degrees of freedom, as observed (Table 1).

The entropy of activation, $\Delta S^\ddagger$, is a measure of the looseness of the TS and is also a reflection of the complexity of the system. $\Delta S^\ddagger$ decreases with increasing size of the cation, from Li^+ to Cs^+, and is larger for the monocomplexes than the bis-complexes. The entropy of activation is largely determined by the molecular parameters used to model the energized molecule and the TS for dissociation but also depends upon the threshold energy. The $\Delta S^\ddagger$(PSL) values at 1000 K are listed in Table 1 and vary between 12 and 61 J/mol·K across these systems. These values are consistent with the loose PSL TS model used to interpret the data.

Theoretical Results. Theoretical structures and energetics for the neutral nMA ligands and for the $M^+(n\text{MA})_x$ complexes, where nMA = NMA and NNDMA, $x = 1$ and 2, and M^+ =

TABLE 1: Fitting Parameters of eq 1, Threshold Dissociation Energies at 0 K, and Entropies of Activation at 1000 K of $M^+(nMA)_x$[a]

complex	σ_0[b]	n[b]	E_0[c] (eV)	E_0(PSL)[b] (eV)	kinetic shift (eV)	$\Delta S^{\ddagger}$(PSL)[b] (J/mol·K)
Li^+(NMA)	11.0 (3.0)	1.8 (0.2)	2.34 (0.12)	2.04 (0.10)	0.30	41 (2)
Na^+(NMA)	5.9 (0.1)	1.1 (0.1)	1.38 (0.04)	1.30 (0.03)	0.08	38 (2)
K^+(NMA)	4.6 (0.3)	1.1 (0.1)	1.03 (0.04)	1.00 (0.04)	0.03	36 (2)
Rb^+(NMA)	4.0 (0.1)	1.5 (0.1)	0.89 (0.03)	0.88 (0.03)	0.01	30 (2)
Cs^+(NMA)	5.8 (0.3)	1.4 (0.0)	0.80 (0.03)	0.79 (0.03)	0.01	26 (2)
$Li^+(NMA)_2$	19.7 (1.7)	1.3 (0.0)	1.67 (0.06)	1.26 (0.05)	0.41	34 (5)
$Na^+(NMA)_2$	51.8 (2.4)	1.1 (0.1)	1.30 (0.05)	1.06 (0.04)	0.24	32 (5)
$K^+(NMA)_2$	62.8 (2.6)	1.4 (0.1)	0.93 (0.05)	0.76 (0.03)	0.17	17 (5)
$Rb^+(NMA)_2$	48.3 (0.5)	1.2 (0.0)	0.91 (0.06)	0.70 (0.02)	0.21	17 (4)
$Cs^+(NMA)_2$	43.7 (2.3)	1.2 (0.1)	0.88 (0.06)	0.67 (0.02)	0.21	17 (5)
Li^+(NNDMA)	15.0 (3.0)	1.8 (0.2)	2.71 (0.09)	2.18 (0.08)	0.53	43 (2)
Na^+(NNDMA)	5.4 (0.2)	1.1 (0.1)	1.52 (0.04)	1.33 (0.04)	0.19	37 (2)
K^+(NNDMA)	2.4 (0.1)	1.1 (0.1)	1.09 (0.04)	1.03 (0.03)	0.06	35 (2)
Rb^+(NNDMA)	6.7 (0.2)	1.1 (0.1)	1.01 (0.04)	0.96 (0.02)	0.05	30 (2)
Cs^+(NNDMA)	4.1 (0.1)	1.3 (0.1)	0.89 (0.04)	0.86 (0.02)	0.03	30 (2)
$Li^+(NNDMA)_2$	56.1 (2.0)	1.0 (0.1)	1.85 (0.04)	1.27 (0.05)	0.58	31 (5)
$Na^+(NNDMA)_2$	69.0 (2.0)	1.1 (0.1)	1.38 (0.06)	1.08 (0.04)	0.30	31 (5)
$K^+(NNDMA)_2$	56.8 (0.6)	0.9 (0.1)	1.20 (0.05)	0.90 (0.03)	0.30	12 (5)
$Rb^+(NNDMA)_2$	39.3 (1.4)	1.2 (0.1)	1.05 (0.05)	0.76 (0.03)	0.29	13 (5)
$Cs^+(NNDMA)_2$	33.4 (1.2)	1.4 (0.1)	1.03 (0.05)	0.73 (0.02)	0.30	13 (5)

[a] Uncertainties are listed in parentheses. [b] Average values for loose PSL TS. [c] No RRKM analysis.

Li^+, Na^+, K^+, Rb^+, and Cs^+, were calculated as described in the Theoretical Calculations section. The BDEs computed for these complexes are listed in Table 2 along with the measured values. For comparison, results for the analogous $M^+(A)_x$ complexes previously studied are also listed.[35] Table 3 provides key geometrical parameters of the ground-state geometries for each of these species.

Electronic Properties of the Neutral *n*MA Ligands. The ground-state geometry-optimized structures of B, A, NMA, and NNDMA are shown in Figure 1 along with their calculated and measured dipole moments and molecular polarizabilities.[36,37] As can be seen in the figure, the overall dipole moment and molecular polarizability of the aromatic ligand increase upon amino substitution and increase further with the extent of methylation. The in-plane (parallel) component of the dipole moment also increases, whereas the perpendicular component decreases with increasing methylation. Both calculated and measured polarizabilities also increase with increasing methylation. Thus, the strength of binding of alkali metal cations to these π-ligands is expected to follow the order NNDMA > NMA > A > B, presuming that the ion−quadrupole and ion−induced-dipole effects dominate the binding as found for π-ligands without a nonzero perpendicular component of the dipole moment. This is explicitly explored below.

Electrostatic potential maps of B, A, NMA, and NNDMA were calculated as described in the Theoretical Calculations section and are shown in Figure 4. Regions of greatest electron density (color-coded in red) occur above and below the plane of the aromatic ring of these ligands as expected for the delocalized π-electron density of the aromatic system. The π-electron density becomes slightly more electronegative upon amino substitution and increases further with the extent of methylation. The most electropositive regions (color-coded in blue) occur around the hydrogen atoms. The region above the amino nitrogen atom of A is of intermediate ESP (green) but becomes increasingly electronegative upon methylation of the amino group (yellow). These ESP maps suggest that a cation should interact most favorably with the π cloud of the aromatic ring. However, interaction with the nitrogen atom of the amino, methylamino, or dimethylamino substituents should also lead to stable binding, albeit of somewhat lower stability.

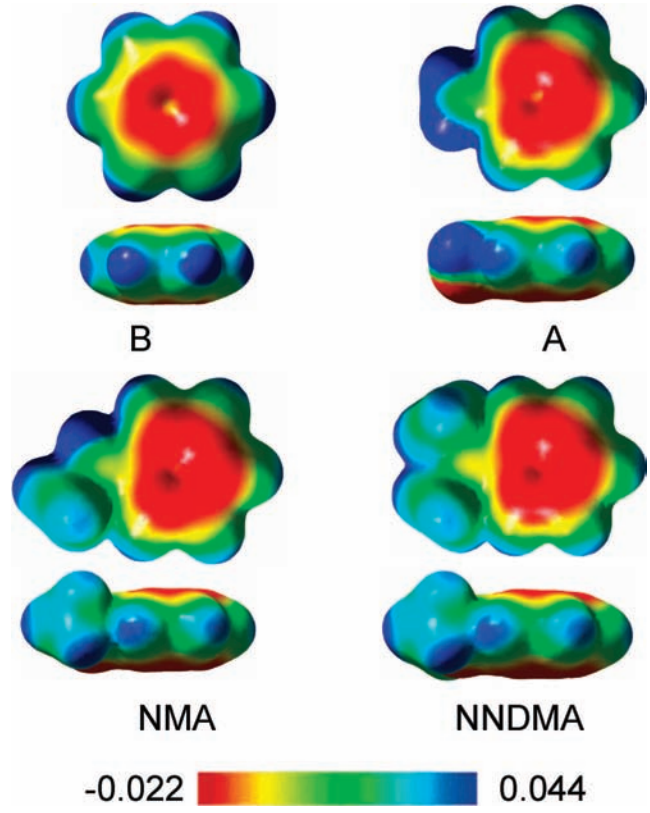

Figure 4. ESP maps of B, A, NMA, and NNDMA at an isosurface of 0.005 au of the total SCF electron density. Two views for each ligand are shown. In the view from above, the molecules are oriented as in Figure 1.

Alkali Metal Cation Binding. Electronic structure calculations reveal that the alkali metal cation prefers to sit directly above the aromatic ring and binds to the π cloud in all of the $M^+(nMA)$ complexes. The geometry-optimized structures of the ground-state conformations of the $Na^+(nMA)$ complexes are shown in Figure 5. In addition to these ground-state conformers, stable conformations in which the cation interacts with the methyl amino or dimethyl amino substituents were also found for the $Li^+(nMA)$, $Na^+(nMA)$, and K^+(NMA) complexes. The

TABLE 2: BDEs of $M^+(nMA)_x$ and $M^+(A)_x$ at 0 K in kJ/mol

	experimental	MP2 Theory			G3 Theory
complex	TCID[a]	D_0[b]	$D_{0,\ BSSE}$[b,c]	D_0[d]	D_0
Li^+(NMA)	196.8 (9.6)	189.2	178.8	183.7	189.9
		173.6[e]	165.3[e]		
Na^+(NMA)	125.0 (3.3)	127.8	117.2		
		120.6[e]	110.8[e]		
K^+(NMA)	96.9 (3.4)	101	94.9		
		95.5[e]	89.4[e]		
Rb^+(NMA)	84.5 (2.6)	85.4[f]	75.0[f]		
Cs^+(NMA)	76.1 (3.0)	77.3[f]	66.9[f]		
$Li^+(NMA)_2$	121.6 (4.7)	145.7	123.9		
$Na^+(NMA)_2$	101.8 (3.4)	112.4	95.8		
$K^+(NMA)_2$	73.1 (2.9)	89.6	78.7		
$Rb^+(NMA)_2$	67.5 (1.9)	87.7[f]	64.6[f]		
$Cs^+(NMA)_2$	64.6 (1.9)	74.5[f]	57.5[f]		
Li^+(NNDMA)	210.3 (7.7)	196.5	186	190.0	195.6
		180.7[e]	171.3[e]		
Na^+(NNDMA)	128.8 (3.7)	132.7	121.9		
		122.9[e]	112.3[e]		
K^+(NNDMA)	99.1 (3.0)	104.5	98.2		
Rb^+(NNDMA)	92.3 (2.3)	88.3[f]	77.4[f]		
Cs^+(NNDMA)	82.8 (2.3)	79.0[f]	68.2[f]		
$Li^+(NNDMA)_2$	122.5 (4.5)	148.6	126.3		
$Na^+(NNDMA)_2$	104.2 (3.8)	115.7	98.8		
$K^+(NNDMA)_2$	86.4 (3.3)	92	80.8		
$Rb^+(NNDMA)_2$	73.3 (2.9)	90.8[f]	66.4[f]		
$Cs^+(NNDMA)_2$	70.4 (1.9)	76.8[f]	59.3[f]		
Li^+(A)	191.5(22.4)[g]	179.7[g]	169.4[g]	174.2	180.7
		168.3[e,g]	160.8[e,g]		
Na^+(A)	119.9 (2.7)[g]	121.5[g]	111.0[g]		
		118.1[e,g]	109.4[e,g]		
K^+(A)	82.5 (3.2)[g]	96.4[g]	90.4[g]		
		93.2[e,g]	87.6[e,g]		
Rb^+(A)	76.3 (4.5)[g]	81.8[f,g]	76.1[f,g]		
		80.8[e,f,g]	73.6[e,f,g]		
Cs^+(A)	69.3 (4.2)[g]	74.5[f,g]	67.4[f,g]		
		72.8[e,f,g]	66.0[e,f,g]		
$Li^+(A)_2$	127.9 (3.7)[g]	144.0[g]	122.5[g]		
$Na^+(A)_2$	98.8 (2.2)[g]	107.9[g]	91.8[g]		
$K^+(A)_2$	75.9 (2.9)[g]	86.5[g]	75.9[g]		
$Rb^+(A)_2$	71.8 (2.7)[g]	81.8[f,g]	70.0[f,g]		
$Cs^+(A)_2$	66.1 (3.3)[g]	66.8[f,g]	57.8[f,g]		

[a] Present results, threshold CID except as noted. [b] Calculated at the MP2(full)/6-311+G(2d,2p) level of theory by using B3LYP/6-31G* optimized geometries. [c] Also includes BSSE corrections. [d] Calculated at the MP2(full)/aug-cc-pVTZ level of theory by using MP2(full)/cc-pVDZ optimized geometries. [e] Cation−π conformer in which the alkali metal cation interacts with the substituent. [f] Hay−Wadt ECP/valence basis set was used for the metal cation, as described in the text. [g] Amunugama and Rodgers, ref 35.

optimized structures of these $Na^+(n$MA) complexes along with their relative stabilities computed at the MP2(full)/6-311+G(2d,2p) level of theory are shown in Figure 5. In these latter conformers, the alkali metal cation lies above the C−N bond and interacts with the π-electron density. Interaction with the π cloud is favored over interaction with the methyl amino and dimethyl amino substituents by 5.0 and 9.6 kJ/mol, respectively, for the complexes to Na^+. Attempts to calculate analogous stable structures for $Rb^+(n$MA$)_x$ and $Cs^+(n$MA$)_x$ always converged to the energetically more favorable ground-state structures in which the alkali metal cation binds to the π cloud of the aromatic ring.

The distortion of the *n*MA ligands that occurs upon complexation to the alkali metal cation is minor. The change in geometry is largest upon binding Li^+ and decreases with increasing size of the alkali metal cation. The distance from the alkali metal cation to the centroid of the aromatic ring and the perpendicular distance to the aromatic ring are found to increase as the size of the alkali metal cation increases for both the $M^+(n$MA) and $M^+(n$MA$)_2$ complexes. These distances are also found to increase on going from the $M^+(n$MA) to the corresponding $M^+(n$MA$)_2$ complex and from the $M^+(NMA)_x$ to the corresponding $M^+(NNDMA)_x$ complex. The metal cation moves away from the amino substituent with increasing methylation for a given alkali metal cation as a result of the increase in the parallel component of the dipole moment.

For the bis-complexes, the most favorable orientation of the two ligands is with the amino substituents anti to each other (i.e., oriented 180° apart). This is shown for the $Na^+(n$MA$)_2$ complexes in Figure 6. To estimate the barrier to free rotation of the *n*MA ligands in the bis-complexes, optimizations were performed for the $Na^+(n$MA$)_2$ complexes with relative orientations of the amino substituents at 0° (syn), 60° (ortho), 90°, 120° (meta), and 180° (anti). The least stable conformation found corresponds to the ligands being oriented syn with respect to one another and are also shown in Figure 6. It can be seen that repulsive interactions between the side chains not directly interacting with the alkali metal cation cause the ligands to fan out from a parallel orientation. This effect is greater for the NNDMA ligands compared to the NMA ligands. Thus, the syn, ortho, 90°, and meta conformations were found to be less stable by 1.1, 0.6, 0.3, and 0.3 kJ/mol, respectively, for $Na^+(NMA)_2$, and by 1.9, 0.7, 0.6, and 0.8 kJ/mol, respectively, for $Na^+(NNDMA)_2$, than when oriented anti. These energies are sufficiently small that at room temperature, the bis-complexes have sufficient internal energy to freely interconvert (see Table 1S in the Supporting Information). The syn structures of the bis-complexes were calculated for all of the metal cations and similar results were obtained.

Conversion from 0 to 298 K. The 0 K BDEs determined here are converted to 298 K bond enthalpies and free energies. The enthalpy and entropy conversions are calculated using standard formulas (assuming harmonic oscillator and rigid rotor models), and the vibrational and rotational constants are determined for the B3LYP/6-31G* optimized geometries and are given in Tables 1S and 2S of the Supporting Information. Table 4 lists 0 and 298 K enthalpies, free energies, and enthalpic and entropic corrections for all systems. The uncertainties in the enthalpic and entropic corrections are determined by 10% variation in the molecular constants for complexes to Li^+, Na^+, and K^+, and by 20% variation in the molecular constants for complexes to Rb^+ and Cs^+. Because the metal−ligand frequencies are very low and may not be adequately described by theory, the listed uncertainties also include contributions from scaling these low-frequency modes up and down by a factor of 2. The latter provides a conservative estimate of the computational errors in these low-frequency modes and is the dominant source of the uncertainties listed. Treatment of the lowest frequency in the bis-ligated systems as a rotor was also considered explicitly but did not change either the enthalpic or entropic corrections.

Discussion

Trends in the Experimental BDEs of $M^+(n$MA$)_x$. The experimental BDEs of the $M^+(n$MA$)_x$ complexes at 0 K are summarized in Table 2. The variation in the measured BDEs with the size of the alkali metal cation is shown in Figure 7 for the mono- and bis-ligated complexes of NMA. Trends are similar for the NNDMA ligand. The M^+−(*n*MA) and (*n*MA)M^+−(*n*MA) BDEs are found to decrease monotonically

TABLE 3: Geometrical Parameters (in Angstroms) of the Optimized Structures of the $M^+(nMA)_x$ Complexes Calculated at the of B3LYP/6-31G* Level

complex	$M^+-\perp$[a]	M^+-R_c[b]	offset[c]	M^+-N	C−C	C−H	C−N	C−NH_3
NMA					1.395	1.080	1.390	1.450
Li^+(NMA)	1.846	1.853	0.158	3.528	1.408	1.080	1.355	1.450
Li^+(NMA)[d]				2.001	1.395	1.082	1.440	1.480
Na^+(NMA)	2.346	2.371	0.304	3.801	1.406	1.080	1.360	1.450
Na^+(NMA)[d]				2.528	1.392	1.082	1.430	1.470
K^+(NMA)	2.824	2.825	0.074	4.010	1.402	1.080	1.370	1.450
K^+(NMA)[d]				2.946	1.394	1.080	1.410	1.470
Rb^+(NMA)	3.123	3.124	0.051	4.197	1.401	1.080	1.380	1.450
Cs^+(NMA)	3.392	3.393	0.080	4.306	1.401	1.080	1.380	1.450
$Li^+(NMA)_2$	2.038	2.052	0.239	3.677	1.404	1.084	1.360	1.456
$Na^+(NMA)_2$	2.404	2.413	0.210	3.861	1.404	1.087	1.372	1.456
$K^+(NMA)_2$	2.883	2.885	0.085	4.066	1.401	1.087	1.379	1.458
$Rb^+(NMA)_2$	3.170	3.170	0.031	4.221	1.401	1.088	1.384	1.458
$Cs^+(NMA)_2$	3.441	3.441	0.060	4.357	1.400	1.085	1.388	1.459
NNDMA					1.395	1.070	1.380	1.440
Li^+(NNDMA)	1.837	1.845	0.161	3.557	1.407	1.080	1.462	1.460
Li^+(NNDMA)[d]				1.998	1.402	1.080	1.450	1.480
Na^+(NNDMA)	2.331	2.339	0.189	3.853	1.407	1.080	1.460	1.460
Na^+(NNDMA)[d]				2.404	1.392	1.082	1.440	1.475
K^+(NNDMA)	2.816	2.821	0.165	4.120	1.404	1.080	1.370	1.460
Rb^+(NNDMA)	3.114	3.118	0.172	4.323	1.404	1.080	1.380	1.460
Cs^+(NNDMA)	3.390	3.393	0.145	4.495	1.404	1.080	1.380	1.460
$Li^+(NNDMA)_2$	2.039	2.058	0.273	3.740	1.404	1.083	1.366	1.460
$Na^+(NNDMA)_2$	2.422	2.434	0.232	3.933	1.404	1.083	1.370	1.459
$K^+(NNDMA)_2$	2.879	2.885	0.178	4.166	1.404	1.083	1.377	1.460
$Rb^+(NNDMA)_2$	3.164	3.169	0.172	4.353	1.404	1.083	1.382	1.460
$Cs^+(NNDMA)_2$	3.440	3.443	0.151	4.535	1.402	1.083	1.385	1.460

[a] Perpendicular distance from the metal cation to the plane of the aromatic ring. [b] Distance from the metal cation to the centroid of the aromatic ring. [c] Parallel distance that the metal cation is offset relative to being positioned over the center of the aromatic ring. [d] Cation−π complexes in which the alkali metal cation interacts with the π-electron density of the substituent.

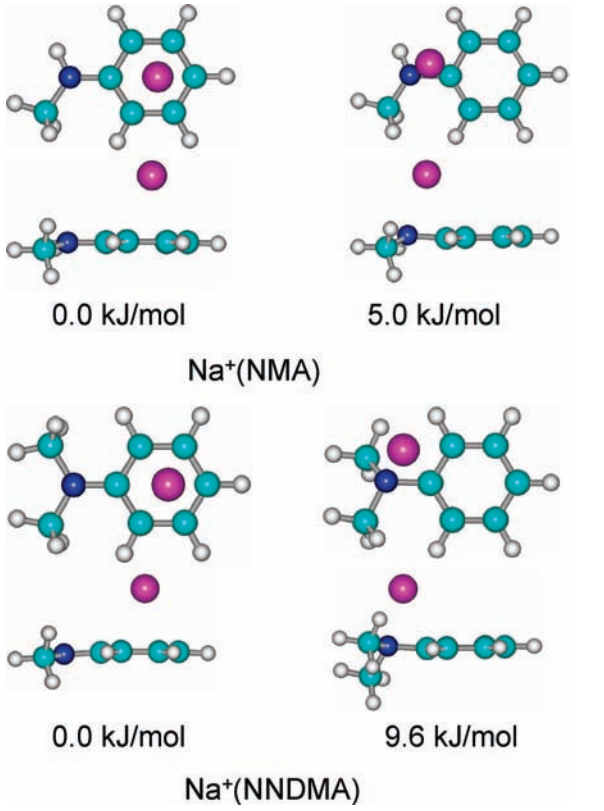

Figure 5. B3LYP/6-31G* optimized geometries and relative MP2(full)/6-311+G(2d,2p) energies at 0 K of the ground-state and low-energy conformers of Na^+(NMA) and Na^+(NNDMA). Two views of each conformer are shown.

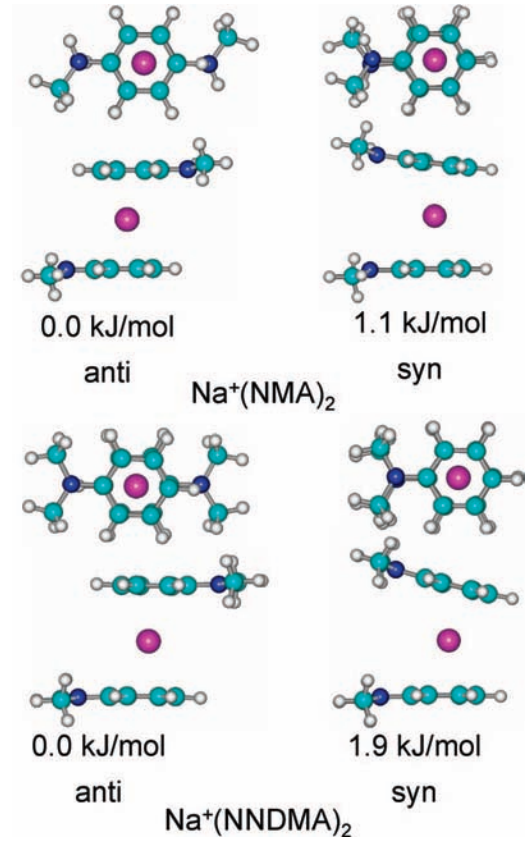

Figure 6. B3LYP/6-31G* optimized geometries of the ground state anti and low-energy syn conformers of $Na^+(NMA)_2$ and $Na^+(NNDMA)_2$. Two views of each conformer are shown.

as the size of the alkali metal cation increases from Li^+ to Cs^+. Similar behavior was also observed for the analogous cation−π complexes to B,[25] T,[26] F,[27] P,[28] S,[29] N,[30] I,[31] R,[32] and A.[35] This is the expected trend for binding based primarily on electrostatic

TABLE 4: Enthalpies and Free Energies of Binding of Ground State $M^+(nMA)_x$ Complexes at 0 and 298 K (kJ/mol)[a]

system	ΔH_0[b]	$\Delta H_{298} - \Delta H_0$[c]	ΔH_{298}	$T\Delta S_{298}$[c]	ΔG_{298}
Li^+(NMA)	196.8 (9.6)	2.7 (0.3)	199.5 (9.6)	30.3 (0.4)	169.2 (9.6)
Na^+(NMA)	125.0 (3.3)	1.0 (0.3)	126.0 (3.4)	30.0 (0.9)	96.0 (3.5)
K^+(NMA)	96.9 (3.4)	0.6 (0.5)	97.5 (3.4)	29.2 (0.9)	68.3 (3.5)
Rb^+(NMA)	84.5 (2.6)	0.2 (0.4)	84.7 (2.6)	27.9 (4.6)	56.8 (5.3)
Cs^+(NMA)	76.1 (3.0)	0.1 (0.8)	76.2 (3.1)	27.1 (1.7)	49.1 (3.5)
$Li^+(NMA)_2$	121.6 (4.7)	−3.6 (1.8)	118.0 (5.0)	40.3 (3.4)	77.7 (6.1)
$Na^+(NMA)_2$	101.8 (3.3)	−3.3 (1.5)	98.5 (3.6)	38.4 (4.0)	60.1 (5.4)
$K^+(NMA)_2$	73.1 (2.9)	−3.3 (1.6)	69.8 (3.3)	34.8 (2.8)	35.0 (4.3)
$Rb^+(NMA)_2$	67.5 (1.9)	−3.3 (1.5)	64.2 (2.4)	34.8 (3.1)	29.4 (3.9)
$Cs^+(NMA)_2$	64.6 (1.9)	−3.3 (2.2)	61.3 (2.9)	44.8 (3.1)	16.5 (4.2)
Li^+(NNDMA)	210.3 (7.7)	2.9 (0.3)	213.2 (7.7)	30.8 (0.8)	182.4 (7.7)
Na^+(NNDMA)	128.8 (3.7)	0.9 (0.3)	129.7 (3.7)	30.0 (0.9)	99.7 (3.9)
K^+(NNDMA)	99.1 (3.0)	0.4 (0.4)	99.5 (3.0)	29.3 (0.9)	70.2 (3.2)
Rb^+(NNDMA)	92.3 (2.3)	0.1 (0.6)	92.4 (2.4)	28.4 (1.5)	64.0 (2.8)
Cs^+(NNDMA)	82.8 (2.3)	0.1 (0.5)	82.9 (2.4)	28.3 (1.4)	54.6 (1.4)
$Li^+(NNDMA)_2$	122.5 (4.5)	−4.1 (3.2)	118.4 (5.5)	39.7 (6.1)	78.7 (8.2)
$Na^+(NNDMA)_2$	104.2 (3.8)	−4.1 (1.9)	100.1 (4.2)	39.7 (6.1)	60.4 (7.4)
$K^+(NNDMA)_2$	86.4 (3.3)	−3.6 (1.2)	82.8 (3.5)	33.9 (2.6)	48.9 (4.4)
$Rb^+(NNDMA)_2$	73.3 (2.9)	−3.6 (1.2)	69.7 (3.1)	33.9 (2.6)	35.8 (4.1)
$Cs^+(NNDMA)_2$	70.4 (1.9)	−3.6 (1.2)	66.8 (2.2)	33.9 (2.6)	32.9 (3.4)

[a] Uncertainties are listed in parentheses. [b] Present TCID results from Table 2. [c] Values from calculations at the MP2(full)/6-311+G(2d,2p) and MP2(full)/HW-6-311+G(2d,2p) levels of theory by using the B3LYP/6-31G* and B3LYP/HW-6-31G* optimized geometries with frequencies scaled by 0.9804.

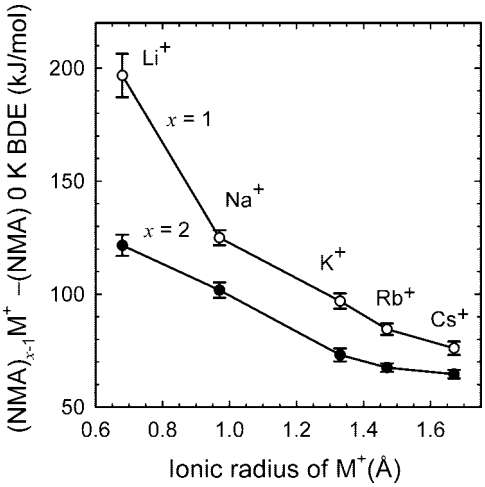

Figure 7. Measured BDEs at 0 K (in kJ/mol) of $M^+(NMA)_x$ complexes plotted versus the ionic radius of M^+.[71] Data are shown for $x = 1$ and 2 and taken from Table 2.

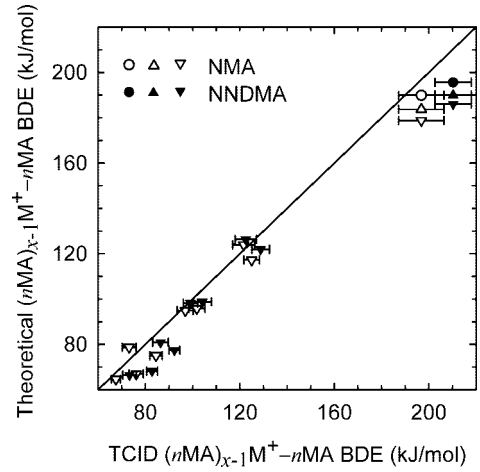

Figure 8. Theoretical MP2(full)/6-311+G(2d,2p) versus experimental 0 K BDEs of $M^+(nMA)_x$, where nMA = NMA and NNDMA, $x = 1$ and 2 (▽ and ▼), and $M^+ = Li^+$, Na^+, K^+, Rb^+, and Cs^+. Values obtained at the MP2(full)/aug-cc-pVTZ and G3 levels of theory for the $Li^+(nMA)$ are also shown as (△ and ▲) and (○ and ●), respectively. The diagonal line indicates the values for which the calculated and measured values are equal.

interactions (ion−dipole, ion−quadrupole, and ion−induced-dipole),[20,70,71] because the increasing size of the alkali metal cation leads to larger metal−ligand bond distances (see Table 3). In general, the BDEs of the $M^+(NNDMA)_x$ complexes are larger than those of the corresponding $M^+(NMA)_x$ complexes because the electron-donating effect of the methyl group increases the electron density above the aromatic ring. Therefore, methylation of aniline leads to an increase in the strength of the cation−π interaction, whereas dimethylation increases the BDEs even further.

The BDEs of the bis-complexes are smaller than the BDEs for the corresponding mono-complexes in all cases. The difference in BDEs is largest for Li^+ and decreases with increasing size of the alkali metal cation. Coulombic and dipole−dipole repulsions between the two ligands lead to this decrease in the sequential BDEs. Larger differences occur for the smaller metal cations as a result of the shorter distance between the two ligands.

Comparison of Theory and Experiment. The experimentally measured and theoretically calculated $(nMA)_{x-1}M^+$−$(nMA)_x$ BDEs at 0 K are summarized in Table 2, and the agreement between the theory and experiment is illustrated in Figure 8. Excellent agreement is found for the $Li^+(nMA)_2$, $Na^+(nMA)_x$, and $K^+(nMA)_x$ complexes, whereas slightly less satisfactory agreement is observed for the complexes to Rb^+ and Cs^+, where ECPs are employed. Poor agreement is found for the $Li^+(nMA)$ complexes. The mean absolute deviation (MAD) for all 20 complexes is 4.9 ± 3.7 kJ/mol, somewhat larger than the average experimental uncertainty, 3.6 ± 1.9 kJ/mol. The MAD for the $M^+(NNDMA)_x$ complexes, 5.5 ± 3.8 kJ/mol, is slightly greater than the MAD for the $M^+(NMA)_x$ complexes, 3.5 ± 3.4 kJ/mol. The MAD for the $M^+(nMA)_2$ complexes, 2.5 ± 2.3 kJ/mol, is smaller than that for the $M^+(nMA)$ complexes, 6.8 ± 3.6 kJ/mol. This largely reflects the lower BDEs of the former complexes.

Inspection of the data makes it clear that the $Li^+(nMA)$ complexes are the principle contributors to the MADs for these

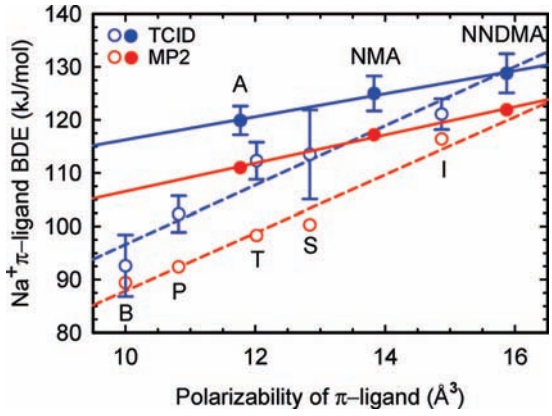

Figure 9. TCID measured (○,●, blue) and MP2(full)/6-311+G(2d,2p) calculated (○,●, red) $Na^+-\pi$-ligand BDEs at 0 K (in kJ/mol) versus the calculated PBE0/6-311+G(2d,2p) polarizability volumes of the π-ligand. Linear regression fits through the data for B, P, T, S, and I and independently for A, NMA, and NNDMA are shown as dashed and solid lines, respectively.

complexes. The explanation for this poorer agreement is that theory systematically underestimates the bond energies for the Li^+ complexes as a result of short Li^+—*n*MA bond distances. Therefore, the aug-cc-pVTZ(Li−C) basis sets were used for the single-point energy calculations with MP2(full) theory for the Li^+(*n*MA) complexes. As explained in the Theoretical Calculation section, the short bond distances in these complexes lead to repulsion between the closed-shell core electrons of Li^+ and the *n*MA ligands. To properly account for such interactions, it is necessary to allow the core electrons to polarize away from the ligand.[55] Using the MP2(full)/aug-cc-pVTZ(Li−C) level for the Li^+(*n*MA) complexes leads to better agreement with experiment. To further explore better theoretical models to accurately describe the binding in Li^+ complexes, G3 calculations were also used to describe these Li^+(*n*MA) complexes. These calculations provide much better agreement with the experimental values. These results are consistent with findings for a large number of other Li^+(ligand) complexes.[55]

Influence of the Polarizability and Dipole Moment of the π-Ligand on the Cation−π Interaction. By comparing the results in this study and those in previous studies of cation−π interactions, a clear and significant substituent effect arising from differences in the electronic properties (i.e., the dipole moments, polarizabilities, and quadrupole moments) of these ligands on the binding strength of the cation−π interaction is found. The variations in the measured and calculated BDEs of cation−π complexes to Na^+ with the calculated polarizabilities are shown in Figure 9. The lines represent independent linear regression fits for the B, P, T, S, and I and A, NMA, and NNDMA ligands, respectively. The increasing polarizability leads to an increase in the strength of the ion−induced-dipole interaction and the overall binding strength between the alkali metal cation and the ligand. Analogous trends are found for the cation−π complexes of the other alkali metal cations.

In earlier work,[26–29,35] we found that the effect of the substituent on the strength of the cation−π interaction could be understood by considering the changes in the quadrupole moment and polarizability of the π-ligand induced by the substituent. As seen in Figure 9, the strength of the cation−π interaction in the complexes to A and NMA is significantly greater than that for complexes to B, P, T, and S and more comparable to I. The main difference between these two ligand groups is the orientation of the dipole moment vector. Whereas B possesses no dipole moment, the dipole moment vectors of P, T, S, and I lie in the plane of the aromatic ring. Therefore, there is no direct ion−dipole contribution to the binding to these ligands. Instead, the dipole moment acts to increase (electron-donating substituents) or decrease (electron-withdrawing substituents) the quadrupole moment and thus the ion−quadrupole interaction. In contrast, A, NMA, and NNDMA all exhibit components of their dipole moments in the direction perpendicular to the plane of the aromatic ring, i.e., along the direction of the cation−π interaction. The perpendicular component of the dipole moment leads to an enhancement in the binding strength of these complexes via an ion−dipole interaction with the metal cation. However, the perpendicular component of the dipole moment decreases with increasing methylation of aniline. Thus, the linear regression line for these ligands does not parallel that for B, P, T, S, and I but rather exhibits a smaller slope, crossing near NNDMA, which has a rather small perpendicular dipole moment.

Nature of the Cation−π Interaction. Noncovalent interactions such as cation−π interactions are the result of a combination of ion−quadrupole, ion−dipole, and ion−induced-dipole interactions. Other interactions, such as dispersion forces or partial covalency, could also contribute but are not included in the analysis because they are either much weaker or essentially a different name for the interactions that are considered. In this study, a detailed numerical analysis was carried out to estimate the relative contributions of these three types of interactions by considering 55 distinct M^+(π-ligand) complexes, where $M^+ = Li^+$, Na^+, K^+, Rb^+, and Cs^+ and π-ligand = B, A, NMA, NNDMA, R, F, P, T, S, N, and I. Previously, Amunugama and Rodgers[30] performed a similar analysis to estimate the relative contributions of the ion−quadrupole and ion−induced-dipole interactions to the binding in cation−π complexes to B, T, A, P, S, F, and N. However, the relative contribution of the ion−dipole and the ion−quadrupole interactions could not be separated by that analysis because A was the only ligand investigated that would have a direct contribution to the binding arising from an ion−dipole interaction. The inclusion of additional π-ligands, NMA and NNDMA, that have ion−dipole contributions to the binding allows the estimation of the individual relative contributions of ion−quadrupole, ion−dipole, and ion−induced-dipole interactions for each complex. This numerical analysis is carried out for both the TCID measured and MP2(full)/6-311+G(2d,2p) theoretical BDEs. The binding parameter model of eq 3 was used for the numerical analysis.

$$\mathrm{BDE}(M^+ - \pi\text{-ligand}) = a(M^+)[Q(\mathrm{B}) + b(M^+)D_{//}(\pi\text{-ligand})] + c(M^+)D_{\perp}(\pi\text{-ligand}) + d(M^+)\alpha(\pi\text{-ligand}) \quad (3)$$

The constants *a*, *b*, *c*, and *d* are fitting constants determined independently for each alkali metal cation (Li^+, Na^+, K^+, Rb^+, and Cs^+). The first term, $a(M^+)[Q(\mathrm{B}) + b(M^+)\ D_{//}(\pi\text{-ligand})]$ represents the contribution of the ion−quadrupole interactions to the binding, where *Q* is the quadrupole moment of B (−8.69 DÅ),[72] the only ligand among this set that has been experimentally determined, and $D_{//}$ is the in-plane (parallel) component of the dipole moment of the π-ligand. The electron-donating (or -withdrawing) effects of the substituent lead to an increase or decrease in the π-electron density of the aromatic ring and thereby enhance (or reduce) the quadrupole moment of the π-ligand. Similarly, the contributions of ion−dipole and

ion−induced-dipole interactions are estimated by the $c(M^+)D_\perp(\pi$-ligand) and $d(M^+)\alpha(\pi$-ligand) terms, respectively, where $D_\perp$ is the perpendicular component of the dipole moment and α is the polarizability volume of each π-ligand. Measured values for the dipole moments of each ligand were used, whereas the parallel and perpendicular components of the dipole moments of A, NMA, and NNDMA were calculated using the measured dipole moments and the dipole orientations obtained from theoretical calculations. Similarly, calculated π-ligand polarizability volumes were used. The measured dipole moments and $D_{//}$, $D_\perp$, and α values for all 11 π-ligands are summarized in Table 3S of the Supporting Information. The absolute and relative contributions of these three cation−π interactions for each $M^+(\pi$-ligand) complex were determined using a weighted analysis of the experimental and theoretical bond energies. (For theory, the uncertainties assumed were 14, 8, 8, 12, and 12 kJ/mol for the complexes to Li^+, Na^+, K^+, Rb^+, and Cs^+, respectively. The values for Li^+ and Na^+ are representative of the uncertainties previously found in comparisons between experiment and theory.[73,74] Values for K^+ were estimated to match those of Na^+, whereas those for Rb^+ and Cs^+ were set higher because of the use of the ECPs.) Initially, the data for all five metal cations were analyzed independently; i.e., 20 parameters (*a*, *b*, *c*, and *d* for each metal cation) were used to reproduce the 55 data points (11 for each metal cation). Overall, this approach reproduces the experimental data with a MAD of 4.2 ± 5.9 kJ/mol and a mean deviation of −1.2 ± 8.1 kJ/mol. Predictions of the theoretical BDEs have a MAD of 2.2 ± 3.5 kJ/mol and a mean deviation of −0.5 ± 4.7 kJ/mol.

One can argue that the term in brackets in eq 3 should not be metal-cation-dependent because this term gives the effective quadrupole moment of each ligand. Thus, the analysis was also performed after replacing the first term by $Q(B) + bD_{//}(\pi$-ligand), thereby utilizing only 16 parameters to reproduce 55 data points. This 16-parameter analysis yields very similar results and predictions as those from the 20-parameter fit, with MADs of 4.5 ± 7.4 and 2.4 ± 3.6 kJ/mol for experimental and theoretical values, respectively. Scrutiny of the results of these two analyses shows strong parallels in the relative contributions of the three cation−π-ligand interactions among the metal cations, suggesting that additional parameters may not be metal-cation-dependent. To test this assumption, the data were analyzed using an 8-parameter fit according to eq 4.

$$\mathrm{BDE}(M^+ - \pi\text{-ligand}) = e(M^+)\{a[Q(B) + bD_{//}(\pi\text{-ligand})] + cD_\perp(\pi\text{-ligand}) + d\alpha(\pi\text{-ligand})\} \quad (4)$$

In this equation, the fitting parameters *a*, *b*, *c*, and *d* are all metal-cation-independent, and the total BDE is scaled for each metal cation using the parameter $e(M^+)$. This yields a family of equivalent fits to the data for which we arbitrarily set $e(Li^+)$ to unity. This method of reproducing both the experimental and theoretical data was again comparable to those of the 16- and 20-parameter analyses, with MADs of 4.7 ± 7.1 and 2.3 ± 1.6 kJ/mol (and mean deviations of −0.4 ± 10.3 and −0.1 ± 3.2 kJ/mol) for experiment and theory, respectively. The overall reproduction of these data with the 8-parameter model is illustrated in Figure 10. Here, it can be seen that the theoretical values are reproduced extremely well using the model, whereas there are a few clear outliers in the plot of the experimental data, notably, $Li^+(C_6H_5F)$, $Li^+(C_6H_5OH)$, and $M^+(C_4H_5N)$ for $M^+ = Na^+$, K^+, Rb^+, and Cs^+. The pyrrole ligand outliers are retained when using the 16- and 20-parameter models. Overall,

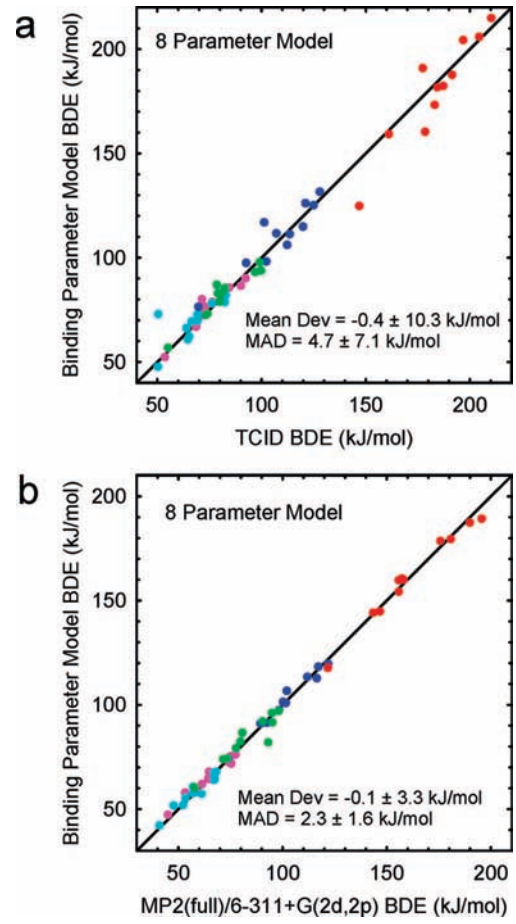

Figure 10. TCID measured (a) and MP2(full)/6-311+G(2d,2p) (b) BDEs versus BDEs predicted by using the 8-parameter model for $M^+(\pi$-ligand) complexes, where $M^+ = Li^+$ (red), Na^+ (blue), K^+ (green), Rb^+ (pink), and Cs^+ (cyan) and π-ligand = B, A, NMA, NNDMA, S, F, P, T, I, R, and N. The diagonal line indicates the values for which the measured (or calculated) and predicted values are equal.

the global analysis of all of the data with the smallest parameter set seems likely to provide the most insight into these interactions and does so with little change in the quality of the reproduction of either the experimental or theoretical data. Therefore, we use the results from the 8-parameter analyses in the following discussion. Parameters from each of the approaches are compiled in Table 4S in the Supporting Information.

The absolute and relative contributions to the cation−π-ligand interactions obtained from the 8-parameter global analysis are listed in Tables 5S and 6S in the Supporting Information for experimental and theoretical BDEs, respectively. The estimated absolute contributions of ion−quadrupole, ion−induced-dipole, and ion−dipole interactions on the M^+−π-ligand complexes are shown in Figure 11. As can be seen in Figure 11a, the ion−quadrupole contribution to the cation−π interaction increases with increasing estimated quadrupole moment of the π-ligand. The ion−induced-dipole contribution to the cation−π interaction also increases with increasing polarizability of the π-ligand (Figure 11b). Ion−dipole contributions to the cation−π interactions are also found to increase with the magnitude of the perpendicular component of the dipole moment as shown in Figure 11c. In all cases, the plots have intercepts at the origin, correctly reflecting the idea that if the quadrupole moment, polarizability, or dipole moment are zero, the contribution to the bond energy should also be zero. The absolute ion−quadrupole, ion−induced-dipole, and ion−dipole contributions to the binding

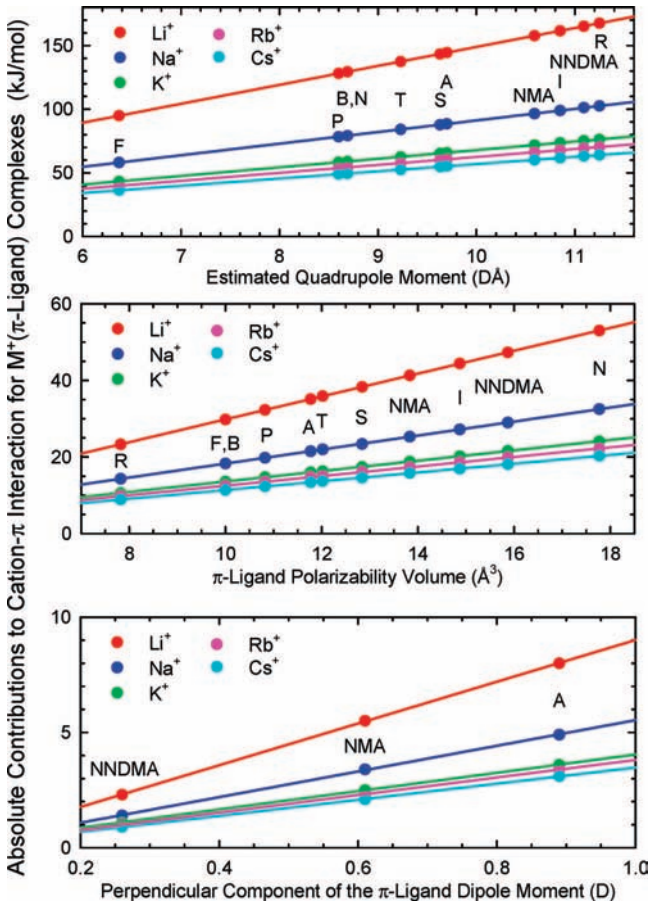

Figure 11. Relative contributions of the ion−quadrupole, ion−dipole, and ion−induced-dipole interactions to the TCID measured BDEs to the cation−π interaction predicted by the 8-binding-parameter model for Na^+(π-ligand) complexes. Ligands are plotted in increasing magnitude of their estimated quadrupole moment, calculated polarizability volume, and perpendicular component of the dipole moment (a−c), respectively.

are expected to decrease with the size of the metal cation for each ligand because the bond distance between the alkali metal cation and the ligand increases with the size of the alkali metal cation, and these interactions scale as R^{-3}, R^{-4}, and R^{-2}, respectively. Indeed, the e parameter of eq 4 shows that the average ratio of the BDEs for Li^+, Na^+, K^+, Rb^+, and Cs^+ is 1.0:0.61:0.46:0.42:0.38 from analyses of the experimental data and 1.0:0.63:0.51:0.40:0.36 from analyses of theoretical BDEs. These are similar to ratios obtained for very different ligands; e.g., the oxygen-based ligands, dimethyl ether, dimethoxy ethane, and 12-crown-4, have ratios for these five metal cations of 1.0:0.63:0.48:0.38:0.29.[75] More extensive data sets for comparing Na^+ to Li^+ and K^+ to Na^+ complexes are also available and give ratios of 0.64 ± 0.06 and 0.72 ± 0.10, respectively.[25–32,75–80] These ratios translate to 1.0:0.64:0.46, in good agreement with the present results.

The results of the binding parameter model analyses find that the binding is dominated by the ion−quadrupole interaction. The experimental values are in the range 76−81% (average of 78 ± 2%) for all ligands except N (71%) and R (88%). Theory provides similar values, with a range of 75−86% (average of 82 ± 4%), except N (78%) and R (91%). For N, the values are low as a consequence of less effective binding to the extended π network because the cation is localized over a single aromatic ring. The π-excessive nature of R, having six π electrons distributed over a five-membered ring rather than over a six-membered ring as for all of the other π-ligands, leads to more effective binding than for all other ligands. Ion−induced-dipole interactions are also found to be important contributors to the binding and account for averages, excluding N and R, of 21 ± 2% and 16 ± 1% of the binding on the basis of the measured and theoretical BDEs, respectively. The N ligand has contributions that are 8 and 6% higher, respectively, whereas the R ligand is lower by 9 and 7%, respectively. For N, the values are high because it is the largest and most polarizable, whereas the values are low for R because it is the smallest and least polarizable of these π-ligands. These changes in the ion−induced-dipole interactions for these two ligands mirror the changes in the ion−quadrupole interactions noted above.

TABLE 5: Estimated Quadrupole Moments of the Neutral π-Ligands (in DÅ)

	estimated quadrupole moment[a]	
ligand	TCID[b]	MP2(full)[c]
A	−9.70 (0.11)	−9.50 (0.12)
NMA	−10.59 (0.21)	−10.21 (0.23)
NNDMA	−11.09 (0.28)	−10.61 (0.30)
S	−9.63 (0.11)	−9.44 (0.12)
F	−6.37 (0.26)	−6.84(0.28)
P	−8.60 (0.01)	−8.62 (0.01)
T	−9.23 (0.06)	−9.12 (0.07)
R	−11.25 (0.29)	−10.74 (0.32)
I	−10.85 (0.24)	−10.41 (0.26)

[a] Uncertainties are listed in parentheses. [b] Values estimated by using TCID measured BDEs. [c] Values estimated by using BDEs computed at the MP2(full)/6-311+G(2d,2p) level of theory for all M^+(π-ligand) complexes except the Li^+(A), Li^+(NMA), and Li^+(NNDMA) complexes, where G3 values are used.

Ion−dipole effects on the binding depend strongly upon the orientation of the molecular dipole moment. The parallel (in-plane) component of the dipole moment serves to increase or decrease the π electron density of the aromatic ring and thus results in an increase or decrease in the strength of the ion−quadrupole interaction. For aromatic ligands with a nonzero perpendicular component of the dipole moment, A, NMA, and NNDMA, ion−dipole interactions also contribute to the binding and account for 4, 3, and 1% of the binding on the basis of the measured BDEs and 11, 7, and 3% of the binding on the basis of the theoretical BDEs. It can also be noted that the ion−perpendicular-dipole interactions appear to reduce the relative contributions of the ion−quadrupole contribution but not the ion−induced-dipole interactions. Thus, the sum of the ion−quadrupole and ion−dipole relative contributions average to 79 ± 2% (experiment) and 84 ± 1% (theory).

The binding parameter model analyses also allow estimates for the quadrupole moments of these π-ligands to be extracted (Table 5). The estimated quadrupole moments for these π-ligands exhibit good agreement with quantitative and semi-quantitative predictions of the influence of the substituent on the π-electron density of the aromatic ring, supporting the validity of the model.

As explained in the Theoretical Calculation section, BDEs for the Li^+(A), Li^+(NMA), and Li^+(NNDMA) complexes calculated using the MP2(full)/aug-cc-pVTZ(Li−C) and G3 levels of theory provide better descriptions of the binding in these complexes. In the 20-parameter analysis, the use of the G3 values also produced better trends in the relative contributions for each type of interaction such that further numerical analyses were carried out including these BDEs instead of MP2(full)/6-311+G(2d,2p) values for the Li^+ complexes. The estimated magnitudes of the Li^+(π-ligand) interactions all

increase slightly when using the G3 values (compared to results obtained using the lower MP2 values), the relative contributions of ion−quadrupole interactions for the Li^+ complexes slightly decreased when using the G3 values, and those for the ion−induced-dipole and ion−dipole interactions increased slightly.

Conclusions

The kinetic energy dependences of the CID of 20 $M^+(n\text{MA})_x$ complexes with Xe are studied by using guided ion beam tandem mass spectrometry, where nMA = *N*-methylaniline and *N*,*N*-dimethylaniline and $x = 1$ and 2. M^+ includes the following alkali metal cations: Li^+, Na^+, K^+, Rb^+, and Cs^+. The dominant pathway for dissociation is the loss of an intact π-ligand. The thresholds for these primary dissociation processes are interpreted to extract 0 and 298 K BDEs. The molecular parameters needed for the analysis of experimental data as well as structures and theoretical estimates for the measured BDEs are determined from calculations performed at the MP2(full)/6-311+G(2d,2p)//B3LYP/6-31G* level of theory. Good agreement is found for the $Li^+(n\text{MA})_2$, $Na^+(n\text{MA})_x$, and $K^+(n\text{MA})_x$ complexes, whereas slightly poorer agreement is observed for the $Rb^+(n\text{MA})_x$ and $Cs^+(n\text{MA})_x$ complexes where ECPs are employed. Poor agreement is found for the $Li^+(n\text{MA})$ complexes, but the agreement improves for calculations performed at higher levels of theory, particularly G3 theory. The absolute $M^+-(n\text{MA})$ and $(n\text{MA})M^+-(n\text{MA})$ BDEs are observed to decrease monotonically as the size of the alkali metal cation increases from Li^+ to Cs^+. Similarly, the difference in the BDEs for the mono- and bis-complexes is also observed to decrease with the size of the alkali metal cation. These trends are explained in terms of the electrostatic nature of the bonding in the $M^+(n\text{MA})_x$ complexes.

The relative contributions of ion−quadrupole, ion−dipole, and ion−induced-dipole interactions to the binding in these complexes as well as estimates for the quadrupole moments for A, NMA, and NNDMA are determined via numerical analysis of the trends in the BDEs for these systems along with previously studied B, P, T, S, F, N, R, and I systems. The estimated quadrupole moments and strength of the ion−quadrupole and ion−induced-dipole interactions are found to increase upon amination and with the extent of methylation. In contrast, ion−dipole interactions increase upon amination but decrease with the extent of methylation of the amino group. For all the complexes (excluding those of N and R), the relative contributions of ion−quadrupole + ion−dipole and ion−induced-dipole interactions to the binding are an average of 79 ± 2% and 21 ± 2%, respectively. The N and R ligands differ systematically from the other ligands because of the differences in the electron density in the aromatic ring. The perpendicular component of the ion−dipole interaction contributes 4, 3, and 1% to the binding for the A, NMA, and NNDMA ligands, respectively. The present results confirm that cation−π interactions are dominated by ion−quadrupole interactions and enhanced by ion−induced-dipole interactions. Ion−dipole contributions to the binding are found for ligands that possess a nonzero component of their dipole moment along the direction of the cation−π interaction but are smaller than the other two contributions.

Acknowledgment. This work is supported by the National Science Foundation, Grants CHE-0518262 (M.T.R.) and CHE-0748790 (P.B.A.), and the American Chemical Society Petroleum Research Fund, Grant 40334-AC6. The authors also thank Wayne State University C&IT for computer time.

Supporting Information Available: Tables of vibrational frequencies and average vibrational energies at 298 K, rotational constants, ligand polarizabilities and dipole moments, fitting parameters of eqs 3 and 4 for all five alkali metal cations and the absolute and relative contributions of the cation−π interactions for all $M^+(\pi\text{-ligand})$ experimental and theoretical BDEs. Figures giving cross sections for CID, thermochemical analyses of zero-pressure extrapolated CID cross sections, and results of the 16 and 20 parameter binding models (PDF). This material is available free of charge via the Internet at http://pubs.acs.org.

References and Notes

(1) Mecozzi, S.; West, A. P., Jr.; Dougherty, D. A. *Proc. Natl. Acad. Sci. U.S.A.* **1996**, *93*, 10566.
(2) Zacharias, N.; Dougherty, D. A. *Trends Pharmacol. Sci.* **2002**, *23*, 281.
(3) Lin, Z.; Johnson, M. E. *FEBS Lett.* **1995**, *370*, 1.
(4) Scrutton, N. S.; Raine, A. R. *Biochem. J.* **1996**, *319*, 1.
(5) Schmitt, J. D.; Sharples, C. G.; Caldwell, W. S. *J. Med. Chem.* **1999**, *42*, 3066.
(6) Kearney, P. C.; Mizoue, L. S.; Kumpf, R. A.; Forman, J. E.; McCurdy, A.; Dougherty, D. A. *J. Am. Chem. Soc.* **1993**, *115*, 9907.
(7) Aoki, K.; Murayama, K.; Nishiyama, H. *J. Chem. Soc. Chem. Commun.* **1995**, *21*, 2221.
(8) Yamada, S.; Morimoto, Y.; Misono, T. *Tetrahedron Lett.* **2005**, *46*, 5673.
(9) Inagaki, Y.; Pham, T. T.; Fujiwara, Y.; Kohno, T.; Osborne, D. A.; Igarashi, Y.; Tigyi, G.; Parrill, A. L. *Biochem. J.* **2005**, *389*, 187.
(10) Kumpf, R. A.; Dougherty, D. A. *Science* **1993**, *261*, 1708.
(11) Satin, J.; Kyle, J. W.; Chen, M.; Bell, P.; Cribbs, L. L.; Fozzard, H. A.; Rogart, R. B. *Science* **1992**, *256*, 1202.
(12) Zhong, W.; Gallivan, J. P.; Zhang, Y.; Li, L.; Lester, H. A.; Dougherty, D. A. *Proc. Natl. Acad. Sci. U.S.A.* **1998**, *95*, 12088.
(13) Cabarcos, O. M.; Weinheimer, C. J.; Lisy, J. M. *J. Chem. Phys.* **1999**, *110*, 8429.
(14) Ryzhov, V.; Dunbar, R. C.; Cerda, B.; Wesdemiotis, C. *J. Am. Soc. Mass Spectrom.* **2000**, *11*, 1037.
(15) Ryzhov, V.; Dunbar, R. C. *J. Am. Chem. Soc.* **1999**, *121*, 2259.
(16) Wintjens, R.; Lievin, J.; Rooman, M.; Buisine, E. *J. Mol. Biol.* **2000**, *302*, 395.
(17) Gallivan, J. P.; Dougherty, D. A. *Proc. Natl. Acad. Sci. U.S.A.* **1999**, *96*, 9459.
(18) Gromiha, M. M.; Santhosh, C.; Suwa, M. *Polymer* **2004**, *45*, 633.
(19) Zhu, D.; Herbert, B. E.; Schlautmn, M. A.; Carraway, E. R.; Hur, J. *J. Environ. Qual.* **2004**, *33*, 1322.
(20) Ma, J. C.; Dougherty, D. A. *Chem. Rev.* **1997**, *97*, 1303.
(21) Mecozzi, S.; West, A. P., Jr.; Dougherty, D. A. *J. Am. Chem. Soc.* **1996**, *118*, 2307.
(22) Orozco, M.; Luque, F. J.; Cubero, E. *Proc. Natl. Acad. Sci. U.S.A.* **1998**, *95*, 5976.
(23) Tsuzuki, S.; Yosida, M.; Uchimaru, T.; Mikami, M. *J. Phys. Chem. A* **2001**, *105*, 769.
(24) Armentrout, P. B.; Rodgers, M. T. *J. Phys. Chem. A* **2000**, *104*, 2238.
(25) Amicangelo, J. C.; Armentrout, P. B. *J. Phys. Chem. A* **2000**, *104*, 11420.
(26) Amunugama, R.; Rodgers, M. T. *J. Phys. Chem. A* **2002**, *106*, 5529.
(27) Amunugama, R.; Rodgers, M. T. *J. Phys. Chem. A* **2002**, *106*, 9092.
(28) Amunugama, R.; Rodgers, M. T. *J. Phys. Chem. A* **2002**, *106*, 9718.
(29) Amunugama, R.; Rodgers, M. T. *Int. J. Mass Spectrom.* **2003**, *222*, 431.
(30) Amunugama, R.; Rodgers, M. T. *Int. J. Mass Spectrom.* **2003**, *227*, 1.
(31) Ruan, C.; Yang, Z.; Hallowita, N.; Rodgers, M. T. *J. Phys. Chem. A* **2005**, *109*, 11539.
(32) Ruan, C.; Yang, Z.; Rodgers, M. T. *Int. J. Mass Spectrom.* **2007**, *267*, 233.
(33) Huang, H.; Rodgers, M. T. *J. Phys. Chem. A* **2002**, *106*, 4277.
(34) Dunbar, R. C.; Klippenstein, S. J.; Yang, C. N.; Gapeev, A. *J. Phys. Chem. A* **2000**, *104*, 3246.
(35) Amunugama, R.; Rodgers, M. T. *Int. J. Mass Spectrom.* **2003**, *227*, 339.
(36) Baysinger, G.; Berger, L. I.; Goldberg, R. N.; Kehiaian, H. V.; Kuchitsu, K.; Rosenblatt, G.; Roth, D. L.; Zwillinger, D.; Lide, D. R. *Handbook of Chemistry and Physics*; CRC Press, Inc: Boca Raton, FL, 2006−2007; Vol. 9−52,53, pp 10−200, 201.
(37) Tucker, S. R.; Walker, S. *J. Chem. Phys.* **1970**, *52*, 2545.
(38) Rodgers, M. T. *J. Phys. Chem. A* **2001**, *105*, 2374.
(39) Ervin, K. M.; Armentrout, P. B. *J. Chem. Phys.* **1985**, *83*, 166.

(40) Muntean, F.; Armentrout, P. B. *J. Chem. Phys.* **2001**, *115*, 1213.
(41) Teloy, E.; Gerlich, D. *Chem. Phys.* **1974**, *4*, 417.
(42) Gerlich, D. Diplomarbeit. University of Freiburg: Federal Republic of Germany, 1971.
(43) Gerlich, D. State-Selected and State-to-State Ion−Molecule Reaction Dynamics, Part I, ExperimentIn *Advances in Chemical Physics Series*; Ng, C.-Y., Baer, M., Eds.; Wiley: New York, 1992; Vol. 82, p 1.
(44) Hales, D. A.; Armentrout, P. B. J. *Cluster Sci.* **1990**, *1*, 127.
(45) Dalleska, N. F.; Honma, K.; Armentrout, P. B. *J. Am. Chem. Soc.* **1993**, *115*, 12125.
(46) Aristov, N.; Armentrout, P. B. *J. Phys. Chem.* **1986**, *90*, 5135.
(47) Dalleska, N. F.; Honma, K.; Sunderlin, L. S.; Armentrout, P. B. *J. Am. Chem. Soc.* **1994**, *116*, 3519.
(48) Frisch, M. J.; Trucks, G. W.; Schlegel, H. B.; Scuseria, G. E.; Robb, M. A.; Cheeseman, J. R.; Montgomery, J. A., Jr.; Vreven, T.; Kudin, K. N.; Burant, J. C.; Millam, J. M.; Iyengar, S. S.; Tomasi, J.; Barone, V.; Mennucci, B.; Cossi, M.; Scalmani, G.; Rega, N.; Petersson, G. A.; Nakatsuji, H.; Hada, M.; Ehara, M.; Toyota, K.; Fukuda, R.; Hasegawa, J.; Ishida, M.; Nakajima, T.; Honda, Y.; Kitao, O.; Nakai, H.; Klene, M.; Li, X.; Knox, J. E.; Hratchian, H. P.; Cross, J. B.; Bakken, V.; Adamo, C.; Jaramillo, J.; Gomperts, R.; Stratmann, R. E.; Yazyev, O.; Austin, A. J.; Cammi, R.; Pomelli, C.; Ochterski, J. W.; Ayala, P. Y.; Morokuma, K.; Voth, G. A.; Salvador, P.; Dannenberg, J. J.; Zakrzewski, V. G.; Dapprich, S.; Daniels, A. D.; Strain, M. C.; Farkas, O.; Malick, D. K.; Rabuck, A. D.; Raghavachari, K.; Foresman, J. B.; Ortiz, J. V.; Cui, Q.; Baboul, A. G.; Clifford, S.; Cioslowski, J.; Stefanov, B. B.; Liu, G.; Liashenko, A.; Piskorz, P.; Komaromi, I.; Martin, R. L.; Fox, D. J.; Keith, T.; Al-Laham, M. A.; Peng, C. Y.; Nanayakkara, A.; Challacombe, M.; Gill, P. M. W.; Johnson, B.; Chen, W.; Wong, M. W.; Gonzalez, C.; Pople, J. A. *Gaussian 03*, revision C.02; Gaussian, Inc.: Wallingford, CT, 2004.
(49) Lee, C.; Yang, W.; Parr, R. G. *Phys. Rev. B* **1998**, *37*, 785.
(50) Becke, A. D. *J. Chem. Phys.* **1993**, *98*, 5648.
(51) The Hay−Wadt valence basis sets and effective core potentials were obtained from the extensible computational chemistry environment basis set Database (available on the Internet at http://www.emsl.pnl.gov/forms/basisform.html), Version 02/25/04, as developed and distributed by the Molecular Science Computing Facility, Environmental and Molecular Sciences Laboratory, which is part of the Pacific Northwest Laboratory, P.O. Box 999, Richland, Washington 99352 and funded by the U.S. Department of Energy. The Pacific Northwest Laboratory is a multi-program laboratory operated by Battelle Memorial Institute for the U.S. Department of Energy under Contract DE-AC06−76RLO 1830.
(52) Hay, P. J.; Wadt, W. R. *J. Chem. Phys.* **1985**, *82*, 299.
(53) Glendening, E. D.; Feller, D.; Thompson, M. A. *J. Am. Chem. Soc.* **1994**, *116*, 10657.
(54) Foresman, J. B.; Frisch, A. E. *Exploring Chemistry with Electronic Structure Methods*; 2nd Ed.; Gaussian: Pittsburgh, 1996; p 64.
(55) Rodgers, M. T.; Armentrout, P. B. *Int. J. Mass Spectrom.* **2007**, *267*, 167.
(56) Dunning, T. H., Jr *J. Chem. Phys.* **1989**, *90*, 1007.
(57) Kendall, R. A.; Dunning, T. H., Jr.; Harrison, R. J. *J. Chem. Phys.* **1992**, *96*, 6796.
(58) Boys, S. F.; Bernardi, R. *Mol. Phys.* **1979**, *19*, 553.
(59) van Duijneveldt, F. B.; van Duijneveldt-van de Rijt, J. G. C. N.; van Lenthe, J. H. *Chem. Rev.* **1994**, *94*, 1873.
(60) Smith, S. M.; Markevitch, A. N.; Romanov, D. A.; Li, X.; Levis, R. J.; Schlegel, H. B. *J. Phys. Chem. A* **2000**, *108*, 11063.
(61) Beyer, T. S.; Swinehart, D. F. *Commum. ACM* **1973**, *16*, 379.
(62) Stein, S. E.; Rabinovitch, B. S. *J. Chem. Phys.* **1973**, *58*, 2438.
(63) Stein, S. E.; Rabinovitch, B. S. *Chem. Phys. Lett.* **1977**, *49*, 183.
(64) Rodgers, M. T.; Ervin, K. M.; Armentrout, P. B. *J. Chem. Phys.* **1997**, *106*, 4499.
(65) Khan, F. A.; Clemmer, D. E.; Schultz, R. H.; Armentrout, P. B. *J. Phys. Chem.* **1993**, *97*, 7978.
(66) Chesnavich, W. J.; Bowers, M. T. *J. Phys. Chem.* **1979**, *83*, 900.
(67) See, for example, Figure 1 in Dalleska, N. F.; Honma, K.; Armentrout, P. B. *J. Am. Chem. Soc.* **1993**, *125*, 12125.
(68) Armentrout, P. B.; Simons, J. *J. Am. Chem. Soc.* **1992**, *114*, 8627.
(69) Rodgers, M. T.; Armentrout, P. B. *J. Phys. Chem. A* **1997**, *101*, 1238.
(70) Rodgers, M. T.; Armentrout, P. B. *Mass Spectrom. Rev.* **2000**, *19*, 215.
(71) Rodgers, M. T.; Armentrout, P. B. *Acc. Chem. Res.* **2004**, *37*, 989.
(72) (a) Williams, J. H. *Acc. Chem. Res.* **1993**, *26*, 593. (b) http://www.chemsoc.org/viselements/pages/data/intro_groupi_data.html.
(73) Armentrout, P. B.; Rodgers, M. T. *J. Phys. Chem. A* **2000**, *104*, 2238.
(74) Rodgers, M. T.; Armentrout, P. B. *Int. J. Mass Spectrom.* **2007**, *267*, 167.
(75) Rodgers, M. T.; Armentrout, P. B. *Mass Spectrom. Rev.* **2000**, *19*, 215.
(76) Moision, R. M.; Armentrout, P. B. *Phys. Chem. Chem. Phys.* **2004**, *6*, 2588.
(77) Yang, Z.; Rodgers, M. T. *J. Am. Chem. Soc.* **2004**, *126*, 16217.
(78) Yang, Z.; Rodgers, M. T. *Int. J. Mass Spectrom.* **2005**, *241*, 225.
(79) Yang, Z.; Rodgers, M. T. *J. Phys. Chem. A* **2006**, *110*, 1455.
(80) Chinthaka, S. D. M.; Rodgers, M. T. *J. Phys. Chem. A* **2007**, *111*, 8152.

JP800434V